Tracking small sensory nerve action potentials in human axonal excitability studies

James Howells[1], Hugh Bostock[2], Susanna B. Park[1], Matthew C. Kiernan[1] and

David Burke[3]

[1]*Brain and Mind Centre, The University of Sydney, Sydney, Australia*

[2]*MRC Centre for Neuromuscular Diseases, National Hospital for Neurology and Neurosurgery, Queen Square, London, UK; and Institute of Neurology, University College London, Queen Square, London, UK*

[3]*Institute of Clinical Neurosciences, Royal Prince Alfred Hospital and the University of Sydney, Sydney, Australia*

Corresponding Author:

James Howells
Brain and Mind Centre
The University of Sydney
94 Mallett St Camperdown
Sydney, NSW 2050
AUSTRALIA.

james.howells@sydney.edu.au

Highlights

- Sensory axons are often more affected than motor in disease. However, the size and latency of the corresponding action potential hampers studies of their properties using threshold tracking.

- This paper addresses these difficulties, with techniques and an amplifier of simple construction. We demonstrate the tracking of 2-µV targets without excessive averaging, and thereby increase the applicability of excitability studies.

- The ability to record sensory potentials in patients with a variety of neuropathic conditions may benefit from the ability to record potentials as small as those recorded here.

Abbreviations

CMAP, compound muscle action potential; CMR(R), common-mode rejection (ratio); CSAP, compound sensory action potential; CTS, carpal tunnel syndrome; EMG, electromyogram; IC, integrated circuit; IV, current-threshold relationship; NCS, nerve conduction study; QT, charge-duration; RC, recovery cycle; TE, threshold electrotonus; SNR, signal-to-noise ratio; SR, Stimulus-response.

49   **Abstract**

50   **Background:** Excitability studies on normal and diseased human axons *in vivo* have been

51   greatly enhanced by fast non-invasive threshold-tracking techniques, using surface

52   stimulation and recording. Although sensory axons are often more affected in disease, most

53   studies to date have focussed on motor axons, because of technical difficulties in resolving

54   pathologically small nerve volleys in the presence of noise and stimulus artefact.

55   **New Methods:** This paper describes techniques for tracking low-amplitude compound

56   action potentials, using a battery-powered, isolated preamplifier of simple construction with

57   high common mode rejection (>125 dB [balanced inputs]) and low noise (<0.4 µV referred to

58   inputs [shorted]).

59   **Results:** We demonstrate the preamplifier's capability by tracking targets as small as 2 µV

60   for a full range of excitability measurements without the usual distortion due to residual

61   stimulus artefact and without the need for clamping, additional filtering or ensemble

62   averaging.

63   **Comparison with existing methods:** In practice, threshold-tracking studies have been

64   unable to study sensory axons when the maximal compound sensory action potential was less

65   than about 15 µV. The techniques and amplifier in the present study allow measurements to

66   be made from nerve with maximal responses less than half that size, and we present three

67   recordings in patients with pathologically small nerve action potentials ≤7µV.

68   **Conclusions:** Based on measurements of stimulus artefact distortion, noise and the

69   performance in experiments, we conclude that the techniques described here will facilitate the

70   study of diseased axons for which the sensory potentials have high thresholds and may be

71   only a few microvolts in amplitude.

1 Introduction

Non-invasive threshold tracking techniques have been applied to the study of the underlying mechanisms of a wide range of neuropathologies (reviewed in: Krarup and Moldovan, 2009; Krishnan et al., 2009). As a rapid *in vivo* method, threshold tracking is able to examine the action of a variety of drugs and toxins in human and animal subjects in real time (Kiernan et al., 2005; Krishnan et al., 2005; Kuwabara and Misawa, 2008; Nodera and Rutkove, 2012; Park et al., 2009).

In contrast to fixed stimulus studies, where the intensity of both conditioning and test stimuli are set and then kept constant, threshold tracking tests the effect of a conditioning stimulus by automatically adjusting the test stimulus intensity to maintain a response at a pre-determined fraction of the maximal compound action potential. This target response is commonly 40-50% of maximum because this lies on the steepest part of the stimulus-response curve.

Even in subjects with only a few surviving motor units, the size and latency of the compound muscle action potential (CMAP) may be sufficient to allow a clean and artefact-free recording. In the study by Kiernan and colleagues (2000) which introduced the technique for the rapid measurement of multiple measures of axonal excitability, and established normative data for clinical testing, the maximal CMAP of thenar muscles to the median nerve stimulation was, on average, 8.4 mV (baseline to peak) and, in a recent report of nerve conduction studies on a large cohort of healthy individuals, it was 9.1 mV with a latency of onset of ~3.6 ms (Benatar et al., 2009).

In contrast excitability studies on sensory axons are technically more challenging, primarily because they depend on nerve action potentials which are much smaller and have shorter latencies (Krarup, 2004). The compound sensory action potential (CSAP) is measured in

95   microvolts and recorded antidromically from the surface with lower limits in relatively young

96   subjects of 26 µV (Kiernan et al., 2001) and 18.1 µV (Howells et al., 2012), when measured

97   peak to peak. However, in 100 normal subjects, Benatar and colleagues (2009) reported the

98   maximal median sensory CSAPs of 3.1 to 86 µV, dependent on age, though the measurement

99   was baseline to peak. In threshold tracking studies, the target potential is submaximal,

100   typically 40 – 50% of the maximal CSAP, so that there may be an inadequate signal-to-noise

101   ratio, in normal subjects, particularly the elderly.

102   Currently there is no commercially available system for electromyography and nerve

103   conduction studies (EMG/NCS) with a real time analogue output suitable for tracking the

104   threshold of sensory axons.

105   In order to track small CSAPs efficiently, the preamplifier requires low noise and high

106   common mode rejection. In addition, for small CSAPs close to the noise level, the threshold

107   tracking strategy needs to take account of the fact that a 'response' may be due to noise alone.

108   This paper shows how a preamplifier of simple construction can be used to track microvolt

109   potentials just above the noise floor established by the recording electrodes, without

110   significant intrusion of the stimulus artefact into the recording. We show how it is possible to

111   study selectively the most excitable sensory axons, well below previously recorded

112   measurements.

113   2   Methods

114   To assess the feasibility of recording axonal excitability with small CSAPs, 14 experiments

115   were performed on three healthy subjects and three subjects with neuropathies resulting in

116   small CSAPs. Recordings of low amplitude targets (~4 µV) were performed on one subject

117   on five separate occasions. All studies were performed with the approval of The University of

118   Sydney's Human Research Ethics Committee, and in conformity with the *Declaration of*

119   *Helsinki*.

2.1   Preamplifier

2.1.1   Design

122   The preamplifier used in this study is illustrated in the Fig. 1 and broadly consists of an input

123   and output stage galvanically separated by an isolation amplifier (ISO124, Burr Brown). The

124   instrumentation amplifier IC (AD8221BR) has exceptional common mode rejection (CMR)

125   and low noise characteristics and the inputs are protected against 1 kV human body model

126   electrostatic discharge (AD8221 datasheet, Analog Devices). High-pass filtering of electrode

127   offsets is achieved by bootstrapping the output by tying the instrumentation amplifier

128   reference to the low-passed output, thereby preserving the high common mode rejection.

129   Universal active filters (UAF42, Texas Instruments) are used to simplify the filter design; the

130   first UAF is configured as a two-pole high-pass (0.2 Hz) Butterworth filter which also

131   provides the low-pass reference signal for the instrumentation amplifier. The second UAF is a

132   two-pole high-pass (2 Hz) Butterworth filter to remove motion artefact. The final pair of

133   UAFs is configured as a four-pole low-pass (2 kHz) Bessel filter, which has superior step

134   response characteristics and is positioned so as to additionally remove the ripple due to the

135   modulation/demodulation carrier frequency of the isolation amplifier. The instrumentation

136   amplifier is configured with a fixed gain of 250 which is suitable for amplification of CMAPs

137   while still achieving good CMR for sensory potentials. Additional gain (x40) for CSAPs is

138   achieved using the auxiliary amplifier of the second UAF. The input and output stages are

139   each powered by a pair of 9-volt (PP3) batteries, and the integrated circuits (ICs) are placed

6

140 so that the current drain is balanced on either side of the isolation. The preamplifier was

141 easily constructed on a single-sided circuit board (100x100 mm) with socketable ICs (apart

142 from the surface mount instrumentation amplifier) and through-hole passive components.

2.1.2 Bench tests

144 The frequency response was tested by applying a 0.5-mV sinusoidal signal to the

145 preamplifier's inputs and measuring the peak response as a function of frequency between 0.2

146 Hz and 10 kHz.

147 The common mode rejection between 10 Hz and 10 kHz was determined by measuring the

148 amplitude of a sinusoidal signal between the preamplifier's inputs (differential-mode, A_{diff})

149 required to give the same output response as a large sinusoidal signal at both inputs

150 (common-mode, A_{cm}). The common mode rejection ratio (CMRR) is calculated as: CMRR =

151 $-20 * \log_{10}(A_{diff}/A_{cm})$.

2.2 Electrodes and skin preparation

153 Skin impedance was lowered at both the recording and stimulation sites by abrasion of the

154 skin surface (3M Trace Prep, 3M, Ontario, Canada), followed by cleaning with an isopropyl

155 alcohol swab. Sensory potentials were first recorded antidromically from digit 2 using

156 disposable Ag/AgCl ring electrodes (RE-D, The Electrode Store, Enumclaw, WA, USA),

157 with two ring electrodes 4 cm apart (Eduardo and Burke, 1988), with the more proximal

158 electrode around the proximal phalanx. The cathode, anode and ground electrodes were of the

159 disposable Ag/AgCl ECG type (1010M & 4620M, Unilect, Unomedical, Stonehouse, UK).

160 The ground electrode was placed on the dorsal aspect of the hand. The cathode was located at

161 the wrist crease with the anode 10 cm proximally, towards the radial edge of the forearm. The

7

162 location of the cathode was adjusted to obtain the minimum threshold current so reducing

163 further the stimulus artefact.

2.3 Excitability testing

165 Axonal excitability was tested with the QtracS threshold tracking software (© Prof Hugh

166 Bostock, Institute of Neurology, UCL, UK) using a stimulus-response paradigm which

167 controlled both the stimulation and recording through a 16-bit multifunction data acquisition

168 device (NI USB-6251).

169 The stimuli were delivered by an isolated bipolar constant current stimulator (DS5, Digitimer,

170 Welwyn Garden City, UK) which followed a real-time command voltage which was

171 synchronised with the recording sweep. The compound action potentials were amplified by

172 the preamplifier (gain x10k) and bandpass filtered (2 Hz to 2 kHz). The amplified waveform

173 had any residual mains frequency noise removed with a HumBug 50/60 Hz noise eliminator

174 (Quest Scientific, North Vancouver, BC, CA) before being digitised at a sampling frequency

175 of 10 kHz.

176 As described in previous studies (Bostock et al., 1998; Howells et al., 2012; Kiernan et al.,

177 2000; Kiernan et al., 2001; Tomlinson et al., 2010) the ***TROND*** protocol cycles through five

178 measures of axonal excitability: stimulus-response (SR) curve, strength-duration relationship

179 (plotted as charge-duration [QT]), threshold electrotonus (TE), current-threshold (IV)

180 relationship and a recovery cycle (RC).

2.4 Tracking small, noisy action potentials

182 For most of the CSAPs recorded, the maximal CSAP and the signal to noise ratio (SNR) were

183 sufficient to allow "proportional tracking" (as in the usual TROND protocol; Kiernan et al.,

184   2000; Kiernan et al., 2001). Proportional tracking adjusts the stimulus step size in proportion

185   to the error between the actual and target responses, allowing fast tracking when the stimulus

186   conditions change rapidly and finer tracking control of the stimulus for slow events. For the

187   smallest CSAPs and noisier recordings, a different tracking strategy was adopted, since the

188   lower SNR meant that proportional tracking would have resulted in excessive oscillations

189   about the target response. A more conservative approach was taken where the basic stimulus

190   step size was a fixed percentage (Δ) of the current stimulus. If successive responses fell on

191   the same side of the target then, the step size was increased by Δ, 2Δ, 3Δ and $4\Delta\%$ of the

192   current stimulus until the target was met (and vice versa). On the other hand, when successive

193   responses fell on opposite sides of the target, the step size was halved until it returned to the

194   basic step size of Δ. This method is referred to as 'arithmetic/geometric tracking'.

195   For low SNR recordings the peak-to-peak measurement accuracy of the biphasic CSAPs was

196   improved by requiring the positive peak to precede the negative peak (i.e. peak[+]-to-peak[-

197   ]).

2.5   Post digitisation signal conditioning

199   Two passes of a 1-2-1 binomial smoothing filter (Marchand and Marmet, 1983) were applied

200   to the digitised data in order to remove high-frequency noise acquired after amplification or

201   as a result of the digitisation process. The transfer function for this low-pass Gaussian filter is

202    $H(f) = \cos^4(\frac{\pi}{2}\frac{f}{f_N})$, where f_N is the Nyquist frequency. Initial observations of the digitised

203   waveforms showed that the stimulus artefacts were small and the return to baseline was

204   nearly complete before the onset of the CSAP. As such, previously required "clamping"

205   techniques were unnecessary, and the measurement window could be shortened (see

206   Discussion).

3 Results

The circuit diagram of the amplifier is shown in Fig. 1A.

3.1 Amplifier performance

With the preamplifier's inputs shorted and the gain set to x10k the output of the preamplifier was measured with a true RMS multimeter (34401A, Agilent) to be 3.85 mV, or 0.385 µV when referred to the amplifier's inputs (RTI). There was no appreciable attenuation in the frequency response of the amplifier between 5 and 1000 Hz (Fig. 1B). Beyond 5 kHz the filter roll-off was 22.3 dB/octave. The high-pass filter has an attenuation of 11 dB/octave below 1 Hz but steepens to 14.9 dB below 0.5 Hz due to the ac-coupling arrangement. The equivalent 'noise bandwidth' was calculated from the frequency response (Fig. 1B) and was 2.4 kHz which gives a noise density of 7.9 nV/$\sqrt{Hz}$ (RTI), in close agreement with the figure in the manufacturer's datasheet.

With balanced inputs the common mode rejection was greater than 136 dB below 500 Hz and had a minimum value of 125 dB (Fig. 1C) over the bandwidth of the amplifier (2 kHz).

3.2 Recovery from stimulus artefact during CSAP recruitment

Figure 2 illustrates the recovery from stimulus artefact during the recruitment of sensory fibres by gradually increasing stimulus strengths. Subject #1 had higher recruitment thresholds (right column) and from the greater stimulus artefact and background noise, most probably a greater skin surface-electrode impedance. The peak deflections due to stimulus artefact were 8.5, 5.2 and 2.2 µV for Subjects #1, 2 and 3 respectively. In all three recordings the stimulus artefact had decayed to a negligible value before the CSAP onset.

3.3 Signal-to-noise measurements *in vivo*

Two passes of the binomial smoothing filter resulted in an additional attenuation of high frequency noise (post-digitisation) with a steep roll off and a -3 dB point at 4.4 kHz (Fig. 1B, open circles).

With the lowest amplitude targets, 10% of CSAP and 2 µV, a measure of the equivalent noise was obtained in one subject (Fig. 3) by sampling the waveform in a window of the same width, but prior to the stimulus (arbitrarily 50 ms earlier than the peak measurement). The noise measured this way was 0.8 ± 0.5 µV (mean $\pm$ SD; closed circles in Fig. 3), not surprisingly the same for both the 10% ($\sim$ 4 µV) and 2-µV targets. The standard deviations for the peak measurements were slightly higher (2 µV, 0.55 µV; 10%, 0.6 µV) reflecting the additional variation in amplitude in response to a tracking stimulus, which is, of necessity, not constant. The vertical bars in Fig. 3 show one standard deviation from the mean measurements. The 10% target and noise are separated by approximately three standard deviations from their means, while the 2-µV target and noise are separated by a little more than one standard deviation.

The signal-to-noise ratio (SNR) was calculated from these data using the formula:

$SNR = \left(\frac{RMS_{peak}}{RMS_{noise}}\right)^2$ giving 19.2 and 5.0 for the 10% and 2-µV targets respectively.

3.4 Threshold tracking small sensory action potentials

3.4.1 Healthy subjects

We found that the smallest practical limit of CSAP size that could be tracked without averaging was 2 µV (except for RC; see Legend to Fig. 4 and Discussion). Using 'arithmetic/geometric' tracking of peak[+]-to-peak[-] amplitudes (see Methods), it was

11

250   possible to obtain all measures of axonal excitability for the 2-µV target in less than 32 min

251   (Fig. 4 [Subject #3], see also Fig. 3B [Subject #2]). The measures from recordings in the

252   three subjects are shown in Fig. 5 (filled circles), and compared with conventional recordings

253   tracking responses 40-50% of maximal in the same subjects (open circles).

254   These recordings suggest that the low-threshold afferents have a greater inward rectification

255   much as in motor axons (Shibuta et al., 2010; Trevillion et al., 2010). However, unlike motor

256   axons there is a suggestion of a relatively depolarized resting membrane potential in these

257   low-threshold sensory axons.

258   3.4.2 Neuropathy

259   Threshold tracking recordings were made in three subjects with neuropathies that resulted in

260   small CSAPs (Kennedy's disease, amyloid neuropathy and chronic inflammatory

261   demyelinating polyneuropathy [CIDP]) as shown in Fig. 6. The maximal CSAPs were:

262   Kennedy's disease, 5.2 µV; amyloid neuropathy, 6.5 µV; and CIDP, 7 µV, and the tracked

263   target CSAPS were 2.1, 2.6, and 2.8 µV, respectively. Recordings of such low-amplitude

264   sensory potentials were not previously possible without averaging many sweeps.

265   3.5 Repeatability of low target recordings

266   Recordings of the 10% target (4.1 ± 0.3 µV) were made in the same subject on five different

267   occasions and are shown in Fig. 7. In the charge-duration plot (QT, Fig 7A) the slope of the

268   lines represents rheobase, and not surprisingly it differs between the individual recordings

269   with differing application of stimulating electrodes. The strength-duration time constant on

270   the other hand was consistent between the recordings (721 ± 22 µs), but longer than the value

271   reported by Kiernan and colleagues (2001) of 527 µs, which was obtained at a target level of

272   40%. Reproducibility of the other excitability recordings was very good, so that the 5 lines

273   for the 5 different recordings can seldom be distinguished.

274   Variability in the recovery cycle recordings is partly due to a reduction in the SNR inherent in

275   the recording technique for the recovery cycle. The response to the supramaximal

276   conditioning stimulus is first subtracted from the conditioned test response before the peak

277   measurement is made, thereby increasing the noise contribution by $\sqrt{2}$, halving the SNR.

278   ## 4   Discussion

279   This paper tackles the difficulty in obtaining reliable measures of the excitability properties

280   of cutaneous sensory axons of low threshold. It is with diseased nerves with pathologically

281   small CSAPs and high thresholds that the true usefulness of the techniques described here

282   may be realised, and the described amplifier has now been used in hundreds of recordings

283   and many of them involving pathologically small CSAPs. The discussion will focus on the

284   optimal recording conditions for small CSAPs, the advantages of the amplifier design, and

285   the physiological and clinical need for better recording techniques.

286   ### 4.1   Axonal excitability close to the electrode noise floor

287   ***Synchronous mains frequency noise*** is to some extent always present in raw biosignals,

288   particularly those acquired from the surface. Notch filters distort action potential

289   measurements and in any case they do not remove the higher harmonics. In-line reduction of

290   mains frequency noise can be achieved in hardware by a device such as the HumBug

291   50/60Hz noise eliminator, or in software by sampling a stimulus free portion of the recording

292   to remove a mains-locked waveform from the response.

293 *Asynchronous noise* due to the impedance of the electrode and skin-electrode interfaces or

294 noise due to the amplification system itself all impact on the signal-to-noise ratio. The

295 amplitude of both synchronous and asynchronous noise can be attenuated by careful skin

296 surface preparation at the recording site and an amplifier with both high common mode

297 rejection and low noise.

298 Because the *stimulus artefact tail* frequently intrudes into the CSAP, so that it rides on the

299 decaying artefact, the standard *TROND* protocol contains a correction for a sloping baseline

300 in CSAPs by "clamping" the digitised data during the measurement window. The sloping

301 baseline is removed by subtracting a straight line that passes through the start and finish of

302 the measurement window at amplitudes corresponding to the mean of the ten samples

303 recorded on either side of the measurement window. This type of clamping assumes that the

304 artefact at the time of the response can be represented as a straight line, whereas it is usually

305 more exponential than linear, so that clamping introduces a systematic and nonlinear

306 distortion of the peak-to-peak measurement. In addition, movement of the CSAP within the

307 measurement window due to changes in its latency alters the amount of distortion. The

308 degree of nonlinearity of the stimulus artefact decay during the measurement window also

309 determines the minimum observable action potential.

310 Alternatives for removing the stimulus artefact after acquisition include artefact subtraction

311 and localised fitting of the baseline; however for threshold tracking of small amplitude

312 potentials these methods have their drawbacks. Artefact subtraction involves the delivery of a

313 fractional stimulus which is subthreshold; the response is then scaled back up to achieve the

314 stimulus artefact alone. Artefact subtraction can be an effective tool for reducing the stimulus

315 artefact (Trevillion et al., 2010); however it doubles the recording time and halves the SNR.

316 Further, because the artefact does not scale linearly with stimulus intensity, the artefact

317 removal is not complete. Another technique is to fit a curve to the decay of the stimulus

318 artefact (Wagenaar and Potter, 2002). Axonal excitability studies, however, involve

319 conditioning the test stimulus with sub- and supra-threshold pulses, in which the conditioning

320 artefact or response may extend beyond the test stimulus.

321 The ***arithmetic/geometric tracking*** applied to the 2-µV potentials in this study, was slower at

322 tracking sharp transitions in stimulus conditions; on the other hand it was less susceptible to

323 noise and overall it resulted in faster tracking of low signal-to-noise-ratio potentials.

324 ***Recovery cycle measurements*** in sensory axons with low SNR were further improved with a

325 hybrid recording protocol. For intervals shorter than 30 ms (which allows for possible M-

326 responses and F-waves), the response to the supramaximal conditioning stimulus needs to be

327 subtracted from the conditioned test. To overcome the resultant halving of the SNR,

328 ensemble averaging of 4 responses was performed for these intervals only (see RC2 in Fig.

329 4).

330 ## 4.2 Conclusion

331 Unlike nerve conduction studies which study the conduction of action potentials along a

332 segment of nerve, threshold tracking studies probe the excitability under the stimulating

333 cathode. The ability to track CSAPs as small as 2 µV opens up the possibility of documenting

334 the properties of nerves and nerve branches not commonly studied, in addition to allowing

335 studies documenting the progression and response to treatment of patients with sensory

336 involvement in polyneuropathies such as kidney disease, (Krishnan et al., 2006), diabetes

337 (Krishnan et al., 2008) and chemotherapy (Park et al., 2011). It is likely that the amplifier will
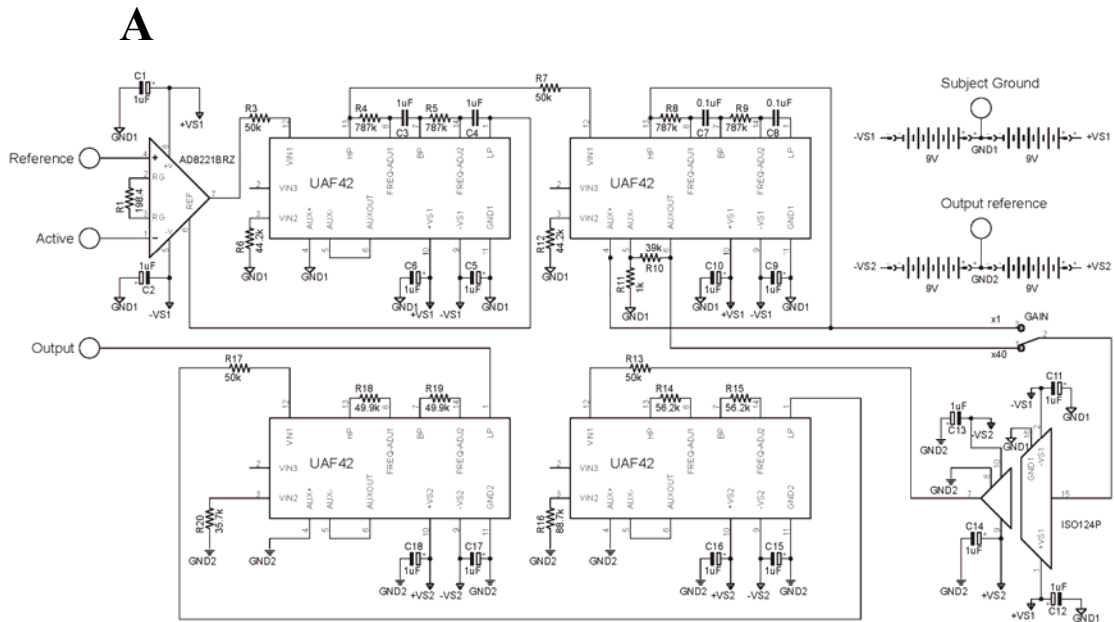
338 be important in clinical trials.

339 **Disclosures**

340   H.B. receives a share of the royalties for the sales of the Qtrac software.
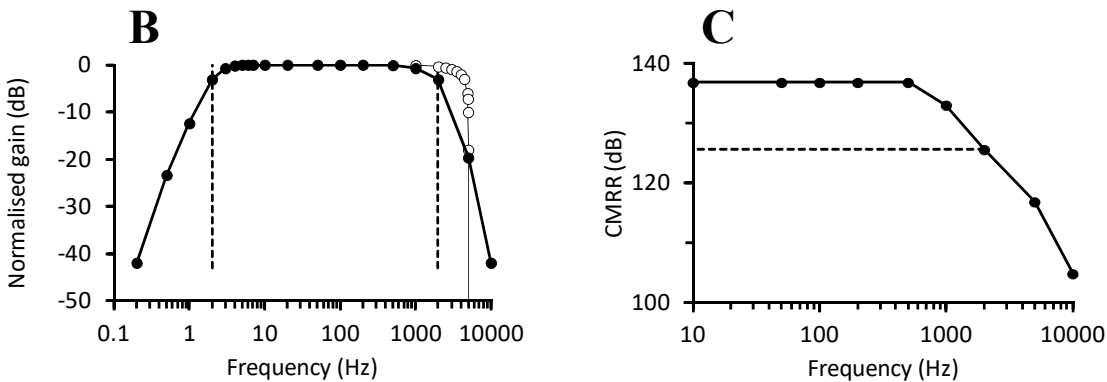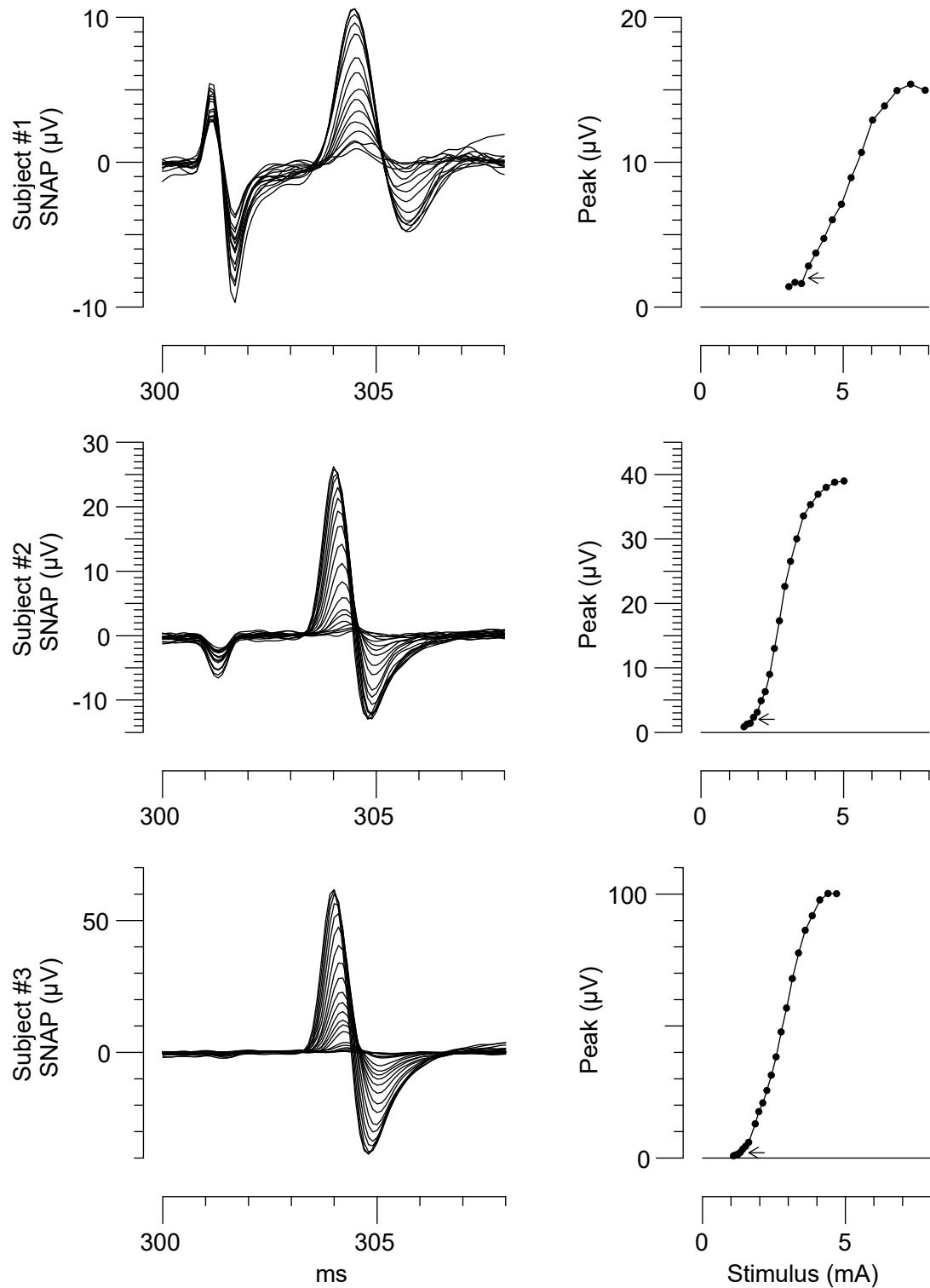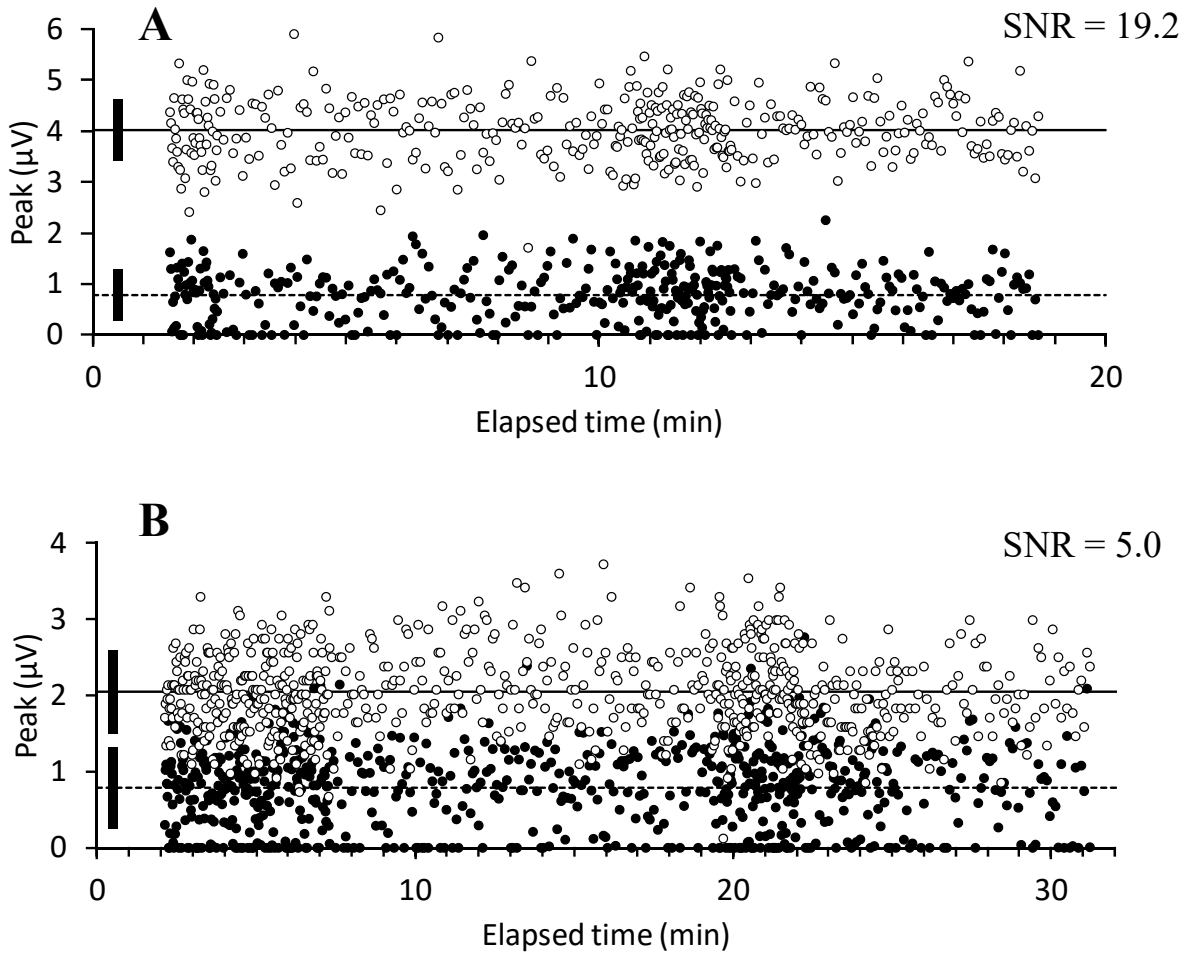
Acknowledgments

347

A

B

C

Figure 1. Battery-powered isolated preamplifier for small sensory potentials.
A. Circuit schematic. The circuit is powered by two pairs of 9-volt batteries and the subject is galvanically isolated from the data acquisition system by the isolation amplifier (ISO124P). The subject ground is tied to the midpoint (GND1) of the pair of batteries on the subject's side of the isolation amplifier, whereas the amplifier's output is referenced to the midpoint (GND2) of the pair of batteries on the data acquisition side of the isolation amplifier. The instrumentation amplifier (AD8221BRZ) provides the critical first stage of amplification and is set to a gain of x250 with a 1% 200Ω resistor (matched as close as possible to 198.4Ω). The first active filter chip decouples any dc-offset potentials. The second active filter is a 2-pole Butterworth high-pass filter (f_c=2Hz) for the removal of motion artefact. The 3rd and 4th active filter chips combined provide a 4-pole low-pass Bessel filter (f_c=2 kHz) to limit the measurement bandwidth. **B.** Normalised frequency response measured with a 0.5-mV sine wave. The gain is normalised to the maximal bandpass response. The dotted lines indicate the band-pass (2 Hz to 2 kHz). The open circles indicate the low-pass filter characteristics of two applications of a 1-2-1 Gaussian filter for data sampled at 10 kHz. **C.** Common mode rejection vs. frequency. The dotted line corresponds to the -3dB frequency of the low pass filter, and shows a minimal CMRR of 125 dB over the amplifier's bandwidth.

367

Figure 2: Recovery from stimulus artefact during CSAP recruitment. Left column.
Averaged CSAP response waveforms to six consecutive stimuli (0.5-ms wide) of
progressively increasing intensity for three subjects. **Right column.** Peak-to-peak
measurements for each of the waveforms in the left column. The arrows indicate the 2-μV
target for each subject.

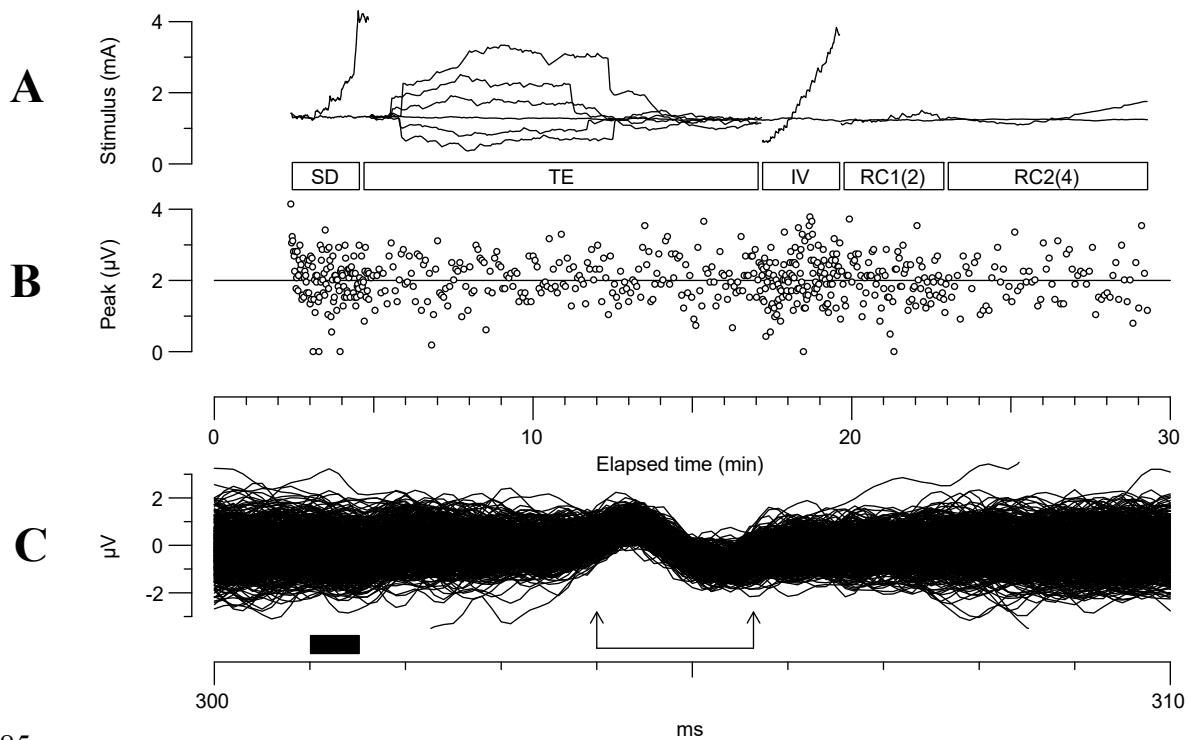**Figure 3: Signal-to-noise ratio (Subject #2 in Fig. 2).** The data represents the peak-to-peak amplitudes of the control channel (unconditioned test; open circles) and the equivalent noise (closed circles). The equivalent noise was measured in an earlier window which preceded the test stimulus. The solid lines indicate the mean amplitude and the dashed lines the mean noise. The vertical bars indicate one standard deviation from the mean. **A.** 10% target (~4 µV) of maximal CSAP. **B.** Target 2 µV. Note that some of the variability in the test data (open circles) is because the stimulus was changing to track the threshold for the target CSAP.
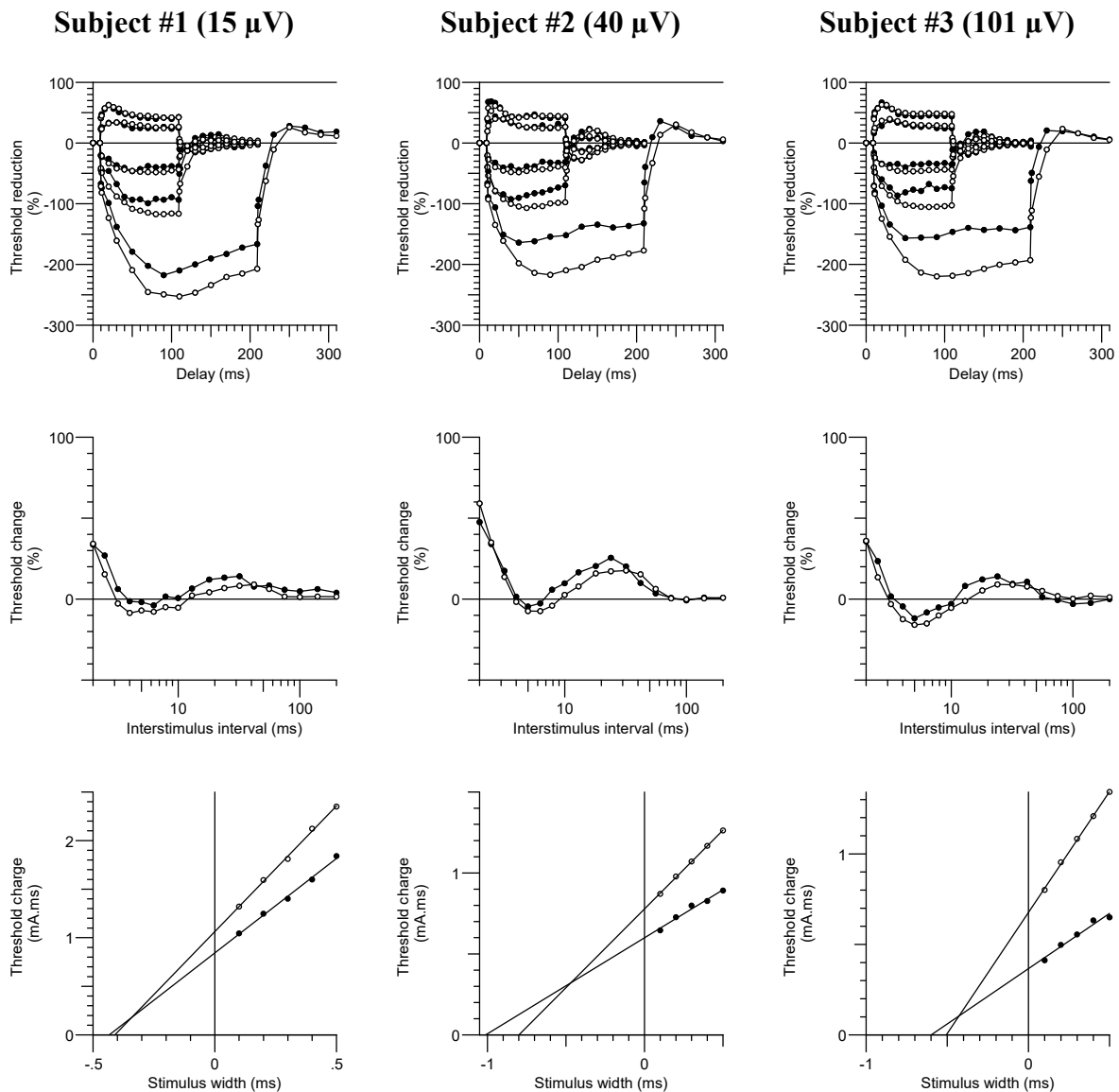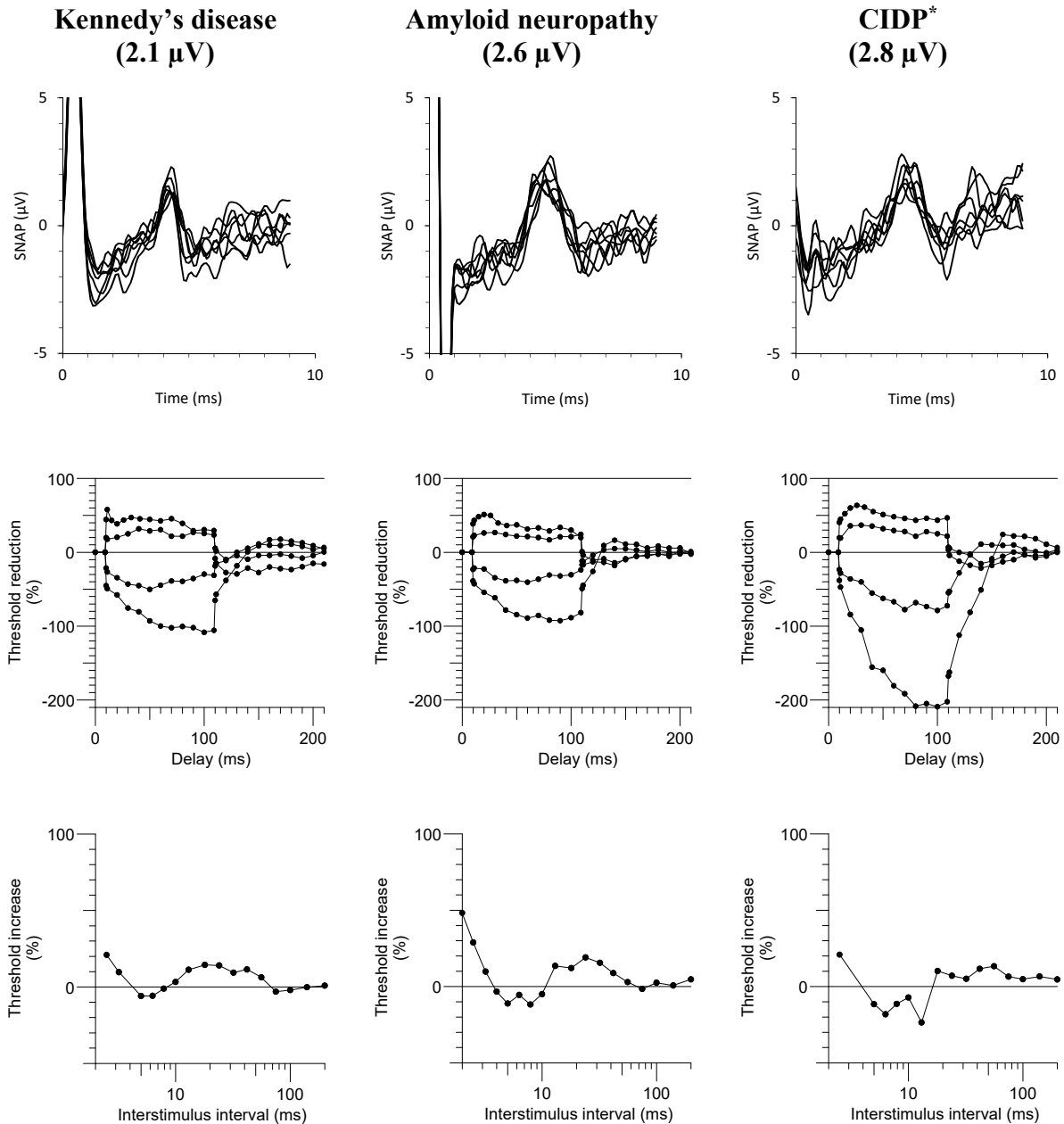
386

387 **Figure 4:** Threshold tracking a 2 µV target potential (Subject #3). The various components
388 of the recording are marked below the data in *A*: SD, strength-duration relationship; TE,
389 threshold electrotonus; IV, current-threshold relationship; RC1, recovery cycle part 1 with 2
390 averages per measurement; RC2, recovery cycle part 2 with subtraction of the response to the
391 conditioning stimulus and with 4 averages per measurement. A. The control stimulus tracked
392 the 2-µV target with a virtually constant value of 1.3 mA for the entire recording. B. The
393 peak-to-peak amplitudes for the unconditioned test potential (2-µV target marked by
394 horizontal line). The variability of the CSAP is due to the intrinsic variability of the recording
395 and the variability of the tracking stimulus. C. Superimposed responses to the unconditioned
396 test stimulus (timing indicated by the solid bar) for the entire recording. Peak-to-peak
397 measurements of the response were made within the interval marked by the arrows, and
398 correspond to the values displayed in *B*.

399

Figure 5: Excitability of low-threshold cutaneous afferents. The maximal CSAP is indicated after the subject. The filled circles denote the low target threshold (2 μV) recordings, and the open circles the standard (40-50%) targets. **Extended threshold electrotonus (top row).** The reduction in threshold to conditioning currents of ±20% and ±40% and -70% of the target threshold. **Recovery cycle (middle row).** The recovery of excitability following a supramaximal stimulus. **Strength-duration properties (bottom row).** Plotted here as charge versus stimulus width. The slope represents rheobase, and not surprisingly is steeper for the standard targets. The absolute value of the X-intercept is the strength-duration time constant, which is longer for the 2-μV targets.
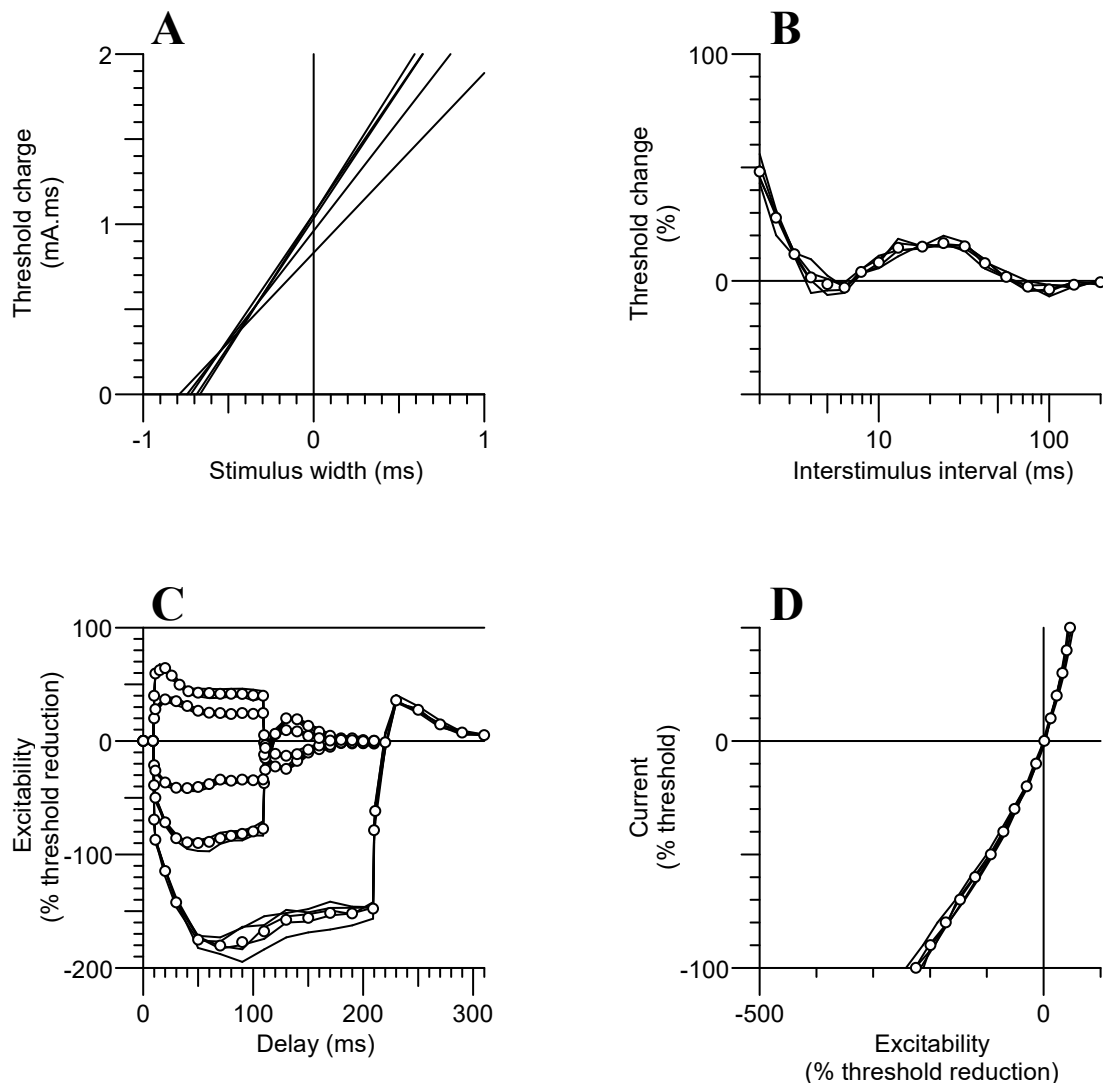
Figure 6: Threshold tracking in patients with neuropathies and pathologically small maximal CSAPs.

Top row: For each patient, 10 consecutive traces of the tracked 40% target potential are shown. The target potential is clearly distinguishable from the background noise.

Middle row: Threshold electrotonus waveforms for each of the neuropathic conditions. The upward deflection at the start of depolarizing threshold electrotonus is probably due inadvertent activation by the conditioning stimulus.

Bottom row: Recovery of excitability following activation by a supramaximal stimulus.

*CIDP = chronic inflammatory demyelinating polyneuropathy

Figure 7: Repeatability of small target recordings (Subject #2). Axonal excitability recordings in the same subject on five different occasions, tracking a 10% CSAP (4.1± 0.3 μV). The open circles represent the mean data and the lines the recordings from different occasions. **A.** Charge-duration plot (QT) of strength-duration properties. The slope of the lines is rheobase, and the X-intercept magnitude corresponds to the strength-duration time constant (SDTC). **B.** The recovery cycle (RC) plots the recovery of an axon following a supramaximal discharge. **C.** Extended threshold electrotonus (TE) recording with conditioning levels of ±20, ±40 and -70% of the unconditioned test threshold. **D.** Current-threshold (IV) relationship plots the threshold reduction versus current strength from +50 to -100% of threshold. *The mean data are not displayed for the QT plot (A), because that may lead to the erroneous interpretation of the X-intercept magnitude as the mean SDTC.*

Figure Legends

Figure 1. Battery-powered isolated preamplifier for small sensory potentials.

A. Circuit schematic. The circuit is powered by two pairs of 9-volt batteries and the subject is galvanically isolated from the data acquisition system by the isolation amplifier (ISO124P). The subject ground is tied to the midpoint (GND1) of the pair of batteries on the subject's side of the isolation amplifier, whereas the amplifier's output is referenced to the midpoint (GND2) of the pair of batteries on the data acquisition side of the isolation amplifier. The instrumentation amplifier (AD8221BRZ) provides the critical first stage of amplification and is set to a gain of x250 with a 1% 200Ω resistor (matched as close as possible to 198.4Ω). The first active filter chip decouples any dc-offset potentials. The second active filter is a 2-pole Butterworth high-pass filter (fc=2Hz) for the removal of motion artefact. The 3rd and 4th active filter chips combined provide a 4-pole low-pass Bessel filter (fc=2 kHz) to limit the measurement bandwidth. **B.** Normalised frequency response measured with a 0.5-mV sine wave. The gain is normalised to the maximal bandpass response. The dotted lines indicate the band-pass (2 Hz to 2 kHz). The open circles indicate the low-pass filter characteristics of two applications of a 1-2-1 Gaussian filter for data sampled at 10 kHz. **C.** Common mode rejection vs. frequency. The dotted line corresponds to the -3dB frequency of the low pass filter, and shows a minimal CMRR of 125 dB over the amplifier's bandwidth.

Figure 2: Recovery from stimulus artefact during CSAP recruitment. Left column. Averaged CSAP response waveforms to six consecutive stimuli (0.5-ms wide) of progressively increasing intensity for three subjects. **Right column.** Peak-to-peak measurements for each of the waveforms in the left column. The arrows indicate the 2-µV target for each subject.

Figure 3: Signal-to-noise ratio (Subject #2 in Fig. 2). The data represents the peak-to-peak amplitudes of the control channel (unconditioned test; open circles) and the equivalent noise (closed circles). The equivalent noise was measured in an earlier window which preceded the test stimulus. The solid lines indicate the mean amplitude and the dashed lines the mean noise. The vertical bars indicate one standard deviation from the mean. **A.** 10% target (~4

464 µV) of maximal CSAP. **B.** Target 2 µV. Note that some of the variability in the test data

465 (open circles) is because the stimulus was changing to track the threshold for the target

466 CSAP.

467

468 **Figure 4: Threshold tracking a 2 µV target potential (Subject #3).** The various

469 components of the recording are marked below the data in *A*: SD, strength-duration

470 relationship; TE, threshold electrotonus; IV, current-threshold relationship; RC1, recovery

471 cycle part 1 with 2 averages per measurement; RC2, recovery cycle part 2 with subtraction of

472 the response to the conditioning stimulus and with 4 averages per measurement. **A.** The

473 control stimulus tracked the 2-µV target with a virtually constant value of 1.3 mA for the

474 entire recording. **B.** The peak-to-peak amplitudes for the unconditioned test potential (2-µV

475 target marked by horizontal line). The variability of the CSAP is due to the intrinsic

476 variability of the recording and the variability of the tracking stimulus. **C.** Superimposed

477 responses to the unconditioned test stimulus (timing indicated by the solid bar) for the entire

478 recording. Peak-to-peak measurements of the response were made within the interval marked

479 by the arrows, and correspond to the values displayed in *B*.

480

481 **Figure 5: Excitability of low-threshold cutaneous afferents.** The maximal CSAP is

482 indicated after the subject. The filled circles denote the low target threshold (2 µV)

483 recordings, and the open circles the standard (40-50%) targets. **Extended threshold**

484 **electrotonus (top row).** The reduction in threshold to conditioning currents of ±20% and

485 ±40% and -70% of the target threshold. **Recovery cycle (middle row).** The recovery of

486 excitability following a supramaximal stimulus. **Strength-duration properties (bottom**

487 **row).** Plotted here as charge versus stimulus width. The slope represents rheobase, and not

488 surprisingly is steeper for the standard targets. The absolute value of the X-intercept is the

489 strength-duration time constant, which is longer for the 2-µV targets.

490

491 **Figure 6: Threshold tracking in patients with neuropathies with pathologically small**

492 **maximal CSAPs.**

493   **Top row:** For each patient, 10 consecutive traces of the tracked 40% target potential are

494   shown. The target potential is clearly distinguishable from the background noise.

495   **Middle row:** Threshold electrotonus waveforms for each of the neuropathic conditions. The

496   upward deflection at the start of depolarizing threshold electrotonus is probably due

497   inadvertent activation by the conditioning stimulus.

498   **Bottom row:** Recovery of excitability following activation by a supramaximal stimulus.

499   *Chronic Inflammatory Demyelinating Polyneuropathy

500

501   **Figure 7: Repeatability of small target recordings (Subject #2).** Axonal excitability

502   recordings in the same subject on five different occasions, tracking a 10% CSAP (4.1± 0.3

503   µV). The open circles represent the mean data and the lines the recordings from different

504   occasions. **A.** Charge-duration plot (QT) of strength-duration properties. The slope of the

505   lines is rheobase, and the X-intercept magnitude corresponds to the strength-duration time

506   constant (SDTC). **B.** The recovery cycle (RC) plots the recovery of an axon following a

507   supramaximal discharge. **C.** Extended threshold electrotonus (TE) recording with

508   conditioning levels of ±20, ±40 and -70% of the unconditioned test threshold. **D.** Current-

509   threshold (IV) relationship plots the threshold reduction versus current strength from +50 to -

510   100% of threshold. *The mean data are not displayed for the QT plot (A), because that may*

511   *lead to the erroneous interpretation of the X-intercept magnitude as the mean SDTC.*

512

References

514 Benatar M, Wuu J, Peng L. Reference data for commonly used sensory and motor nerve conduction
515 studies. Muscle & nerve, 2009; 40: 772-94.

516 Bostock H, Cikurel K, Burke D. Threshold tracking techniques in the study of human peripheral nerve.
517 Muscle & nerve, 1998; 21: 137-58.

518 Eduardo E, Burke D. The optimal recording electrode configuration for compound sensory action
519 potentials. Journal of neurology, neurosurgery, and psychiatry, 1988; 51: 684-7.

520 Howells J, Trevillion L, Bostock H, Burke D. The voltage dependence of I(h) in human myelinated
521 axons. The Journal of physiology, 2012; 590: 1625-40.

522 Kiernan MC, Burke D, Andersen KV, Bostock H. Multiple measures of axonal excitability: a new
523 approach in clinical testing. Muscle & nerve, 2000; 23: 399-409.

524 Kiernan MC, Isbister GK, Lin CS-Y, Burke D, Bostock H. Acute tetrodotoxin-induced neurotoxicity after
525 ingestion of puffer fish. Annals of neurology, 2005; 57: 339-48.

526 Kiernan MC, Lin CS-Y, Andersen KV, Murray NM, Bostock H. Clinical evaluation of excitability
527 measures in sensory nerve. Muscle & nerve, 2001; 24: 883-92.

528 Krarup C. Compound sensory action potential in normal and pathological human nerves. Muscle &
529 nerve, 2004; 29: 465-83.

530 Krarup C, Moldovan M. Nerve conduction and excitability studies in peripheral nerve disorders.
531 Current opinion in neurology, 2009; 22: 460-6.

532 Krishnan AV, Goldstein D, Friedlander M, Kiernan MC. Oxaliplatin-induced neurotoxicity and the
533 development of neuropathy. Muscle & nerve, 2005; 32: 51-60.

534 Krishnan AV, Lin CS-Y, Kiernan MC. Activity-dependent excitability changes suggest Na+/K+ pump
535 dysfunction in diabetic neuropathy. Brain : a journal of neurology, 2008; 131: 1209-16.

536 Krishnan AV, Lin CS-Y, Park SB, Kiernan MC. Axonal ion channels from bench to bedside: a
537 translational neuroscience perspective. Progress in neurobiology, 2009; 89: 288-313.

538 Krishnan AV, Phoon RK, Pussell BA, Charlesworth JA, Kiernan MC. Sensory nerve excitability and
539 neuropathy in end stage kidney disease. Journal of neurology, neurosurgery, and psychiatry, 2006;
540 77: 548-51.

541 Kuwabara S, Misawa S. Pharmacologic intervention in axonal excitability: in vivo assessment of nodal
542 persistent sodium currents in human neuropathies. Current molecular pharmacology, 2008; 1: 61-7.

543 Marchand P, Marmet L. Binomial smoothing filter: A way to avoid some pitfalls of least squares
544 polynomial smoothing. Review of scientific instruments, 1983; 54: 1034-41.

545 Nodera H, Rutkove SB. Changes of the peripheral nerve excitability in vivo induced by the persistent
546 Na+ current blocker ranolazine. Neuroscience letters, 2012; 518: 36-40.

547 Park SB, Lin CS-Y, Krishnan AV, Goldstein D, Friedlander ML, Kiernan MC. Dose effects of oxaliplatin
548 on persistent and transient Na+ conductances and the development of neurotoxicity. PloS one,
549 2011; 6: e18469.

550 Park SB, Lin CS-Y, Krishnan AV, Goldstein D, Friedlander ML, Kiernan MC. Oxaliplatin-induced
551 neurotoxicity: changes in axonal excitability precede development of neuropathy. Brain : a journal of
552 neurology, 2009; 132: 2712-23.

553 Shibuta Y, Nodera H, Mori A, Okita T, Kaji R. Peripheral nerve excitability measures at different target
554 levels: the effects of aging and diabetic neuropathy. Journal of clinical neurophysiology : official
555 publication of the American Electroencephalographic Society, 2010; 27: 350-7.

556 Tomlinson S, Burke D, Hanna M, Koltzenburg M, Bostock H. In vivo assessment of HCN channel
557 current (I(h)) in human motor axons. Muscle & nerve, 2010; 41: 247-56.

558 Trevillion L, Howells J, Bostock H, Burke D. Properties of low-threshold motor axons in the human
559 median nerve. The Journal of physiology, 2010; 588: 2503-15.

560 Wagenaar DA, Potter SM. Real-time multi-channel stimulus artifact suppression by local curve
561 fitting. Journal of neuroscience methods, 2002; 120: 113-20.

562